J Electr Eng Technol.2015;10(1): 280-287
http://dx.doi.org/10.5370/JEET.2015.10.1.280

ISSN(Print) 1975-0102
ISSN(Online) 2093-7423

Current Decoupling Control for the Three-level PWM Rectifier with a Low Switching Frequency

Qing-qing YUAN† and Kun XIA*

Abstract – Three-level PWM rectifiers applied in medium voltage applications usually operate at low switching frequency to keep the dynamic losses under permitted level. However, low switching frequency brings a heavy cross-coupling between the current components i_d and i_q with a poor dynamic system performance and a harmonic distortion in the grid-connecting current. To overcome these problems, a mathematical model based on complex variables of the three-level voltage source PWM rectifier is firstly established, and the reasons of above issues resulted from low switching frequency have been analyzed using modern control theory. Then, a novel control strategy suitable for the current decoupling control based on the complex variables for i_d and i_q is designed here. The comparisons between this kind of control strategy and the normal PI method have been carried out. MATLAB and experimental results are given in detail.

Keywords: Three-level PWM rectifier, Low switching frequency, Cross-coupling, Complex current controller

1. Introduction

Nowadays, PWM rectifiers have been widely applied in series of industrial fields, such as Static Reactive Power Generator (SVG), Active Power Filter (APF), Unified Power Flow Controller (UPFC), High Voltage DC Transmission (HVDC) and some renewable energy generation system [1-6]. The key issues concerning the control of a three-level voltage source PWM rectifier are about neutral potential balancing, switch losses and the cross-coupling between i_d and i_q. In order to improve the output power of the converters, the switching frequency of the semi-conductors (IGBT, IGCT or GTO) are usually kept low to restrain switch losses at permitted level [7-9]. However, low switching frequency not only brings about a heavy cross-coupling between the current components i_d and i_q as well as a poor dynamic system performance [10, 11], also a severe harmonic distortion, especially the low order harmonics, in the grid-connecting current [12].

Considering the situation that rectifiers usually being connected to grid, a heavy harmonic distortion can't meet the grid standards, and will be harmful to other grid loads. A novel dead beat control scheme combining with repetitive control was presented in [13], while it didn't take consideration of the influence of low switching frequency. Literature [14] put forward a model predictive control strategy in static coordinates, which had a nice performance with a low switching frequency, however, its characteristic of frequency fluctuation brought about some other difficulties in filter design and issues of electro-magnetic compatibility. Two kinds of approaches have been proposed in [15] to improve the harmonic distortion resulted from low switching frequency, in which a LCL filter was considered, whose reasonable parameters and volume could be a problem for its development.

Studies on a novel control scheme for a high-power three-level voltage source PWM rectifier with a low switching frequency have been carried out in this paper, which are focusing on current decoupling controller. Section 2 establishes a complex model with low switching frequency for a three-level PWM rectifier case considered in this paper, and Section 3 analyze the problems resulted from low switching frequency in detail. Section 4 describes a novel complex current controller to realize the decoupling between i_d and i_q, along with some simulation verification. The whole control scheme is shown in Section 5 and the performance are evaluated based on a experimental platform whose microprocessor being DSP and FPGA, at switching frequency f_s=500Hz.

2. Complex Model for Three-level PWM Rectifier

The topology of a three-level PWM voltage source rectifier studied in this paper is shown in Fig. 1.

Where, e_a, e_b, e_c represent the grid voltages; i_a, i_b and i_c are grid-side currents; v_{aO}, v_{bO}, v_{cO} are ac voltages; L and R are the filter inductance and resistance respectively; R_L stands for load while i_L is the load current; i_{dc} is the current of DC-link and V_{dc} represents the DC-link voltage; C_1 and C_2 are DC-link capacitors whose voltages are u_{c1} and u_{c2}; O

† Corresponding Author: Dept. of Optical-Electrical and Computer Engineering, University of ShangHai for Science and Technology, China. (cumtxz1215@163.com)
* Dept. of Optical-Electrical and Computer Engineering, University of ShangHai for Science and Technology, China.
Received: January 12, 2014; Accepted: September 24, 2014

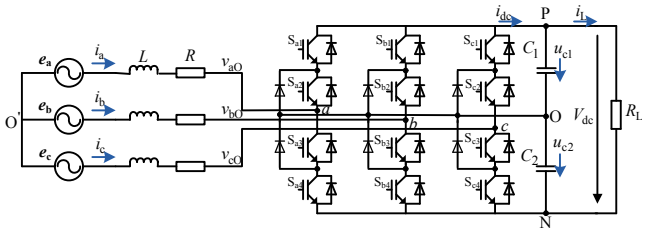

Fig. 1. Topology of the three-level PWM voltage source rectifier

stands for clamped point while O' is the midpoint of the grid.

The traditional models for PWM rectifier are described in dq coordinates as following

$$\begin{cases} L\dfrac{\mathrm{d}i_\mathrm{d}}{\mathrm{d}t} + Ri_\mathrm{d} - \omega_\mathrm{s} L i_\mathrm{q} + v_\mathrm{d} = e_\mathrm{d} \\ L\dfrac{\mathrm{d}i_\mathrm{q}}{\mathrm{d}t} + Ri_\mathrm{q} + \omega_\mathrm{s} L i_\mathrm{d} + v_\mathrm{q} = e_\mathrm{q} \end{cases} \tag{1}$$

$$\begin{aligned} v_\mathrm{d} &= \mathrm{S}_\mathrm{dP} u_\mathrm{c1} + \mathrm{S}_\mathrm{dN} u_\mathrm{c2} \\ v_\mathrm{q} &= \mathrm{S}_\mathrm{qP} u_\mathrm{c1} + \mathrm{S}_\mathrm{qN} u_\mathrm{c2} \end{aligned} \tag{2}$$

Where, e_d and e_q are the dq components of the grid voltage; v_d, v_q represent the dq components of the ac voltage respectively and i_d, i_q are the grid-side currents in dq coordinates; p is differential operator; ω_s stands for grid angular frequency and S_dP, S_qP, S_dN, S_qN represent the switch status also in dq coordinates.

Defining complex variables as

$$\begin{aligned} \boldsymbol{i}_\mathrm{s} &= i_\mathrm{d} + \mathrm{j}i_\mathrm{q} \\ \boldsymbol{v}_\mathrm{s} &= v_\mathrm{d} + \mathrm{j}v_\mathrm{q} \\ \boldsymbol{e}_\mathrm{s} &= e_\mathrm{d} + \mathrm{j}e_\mathrm{q} \\ \mathbf{S}_\mathrm{P} &= \mathrm{S}_\mathrm{dP} + \mathrm{j}\mathrm{S}_\mathrm{qP} \\ \mathbf{S}_\mathrm{N} &= \mathrm{S}_\mathrm{dN} + \mathrm{j}\mathrm{S}_\mathrm{qN} \end{aligned} \tag{3}$$

With the definitions in Eq. (3), the complex models can be obtained without the consideration of the influence of switching frequency

$$\begin{aligned} &\tau_\mathrm{s}\frac{d\boldsymbol{i}_\mathrm{s}}{dt} + \boldsymbol{i}_\mathrm{s} + \mathrm{j}\omega_\mathrm{s}\tau_\mathrm{s}\boldsymbol{i}_\mathrm{s} = (\boldsymbol{e}_\mathrm{s} - \boldsymbol{v}_\mathrm{s})/R \\ &\boldsymbol{v}_\mathrm{s} = \mathbf{S}_\mathrm{P} u_\mathrm{c1} + \mathbf{S}_\mathrm{N} u_\mathrm{c2} \end{aligned} \tag{4}$$

Where, $\tau_\mathrm{s} = L/R$ is the time constant of the ac side; $\boldsymbol{e}_\mathrm{s}$, $\boldsymbol{i}_\mathrm{s}$, $\boldsymbol{v}_\mathrm{s}$ are the complex variables of grid voltage, grid-side current and ac voltage respectively; $\mathbf{S}_\mathrm{P}$ and $\mathbf{S}_\mathrm{N}$ are complex variables about the switch statuses.

From Eq. (4), the complex transform of the current loop can be obtained as

$$\boldsymbol{F}_\mathrm{vsr}(s) = \frac{1/R}{\tau_\mathrm{s}s + 1 + \mathrm{j}\omega_\mathrm{s}\tau_\mathrm{s}} \tag{5}$$

A low switching frequency influence the control system in terms of an effect on the PWM link and we use Eq. (6) to make an approximation, which containing a cross-coupling factor $\mathrm{j}\omega_\mathrm{s}\tau_\mathrm{d}\boldsymbol{v}_\mathrm{s}$.

$$\tau_\mathrm{d}\frac{\mathrm{d}\boldsymbol{v}_\mathrm{s}}{\mathrm{d}t} + (1 + \mathrm{j}\omega_\mathrm{s}\tau_\mathrm{d})\boldsymbol{v}_\mathrm{s} = \boldsymbol{v}_\mathrm{s}^* \tag{6}$$

While, $\boldsymbol{v}^*_\mathrm{s}$ is the reference voltage vector resulted from the current controller; τ_d stands for the delay time with the low switching frequency and the sampling delay, normally,τ_d=0.75/f_s (f_s is switching frequency) [11,16]. And the complex transform of Eq. (6) is

$$\boldsymbol{F}_\mathrm{d}(s) = \frac{\boldsymbol{V}_\mathrm{s}(s)}{\boldsymbol{V}_\mathrm{s}^*(s)} = \frac{1}{\tau_\mathrm{d}s + 1 + \mathrm{j}\omega_\mathrm{s}\tau_\mathrm{d}} \tag{7}$$

The complex transform of the whole current loop can written as

$$\begin{aligned} \boldsymbol{F}_\mathrm{m}(s) &= \boldsymbol{F}_\mathrm{vsr}(s)\boldsymbol{F}_\mathrm{d}(s) \\ &= 1/R \cdot \frac{1}{\tau_\mathrm{s}s + 1 + \mathrm{j}\omega_\mathrm{s}\tau_\mathrm{s}} \frac{1}{\tau_\mathrm{d}s + 1 + \mathrm{j}\omega_\mathrm{s}\tau_\mathrm{d}} \end{aligned} \tag{8}$$

3. Cross-coupling Problem with a Low Switching Frequency

The corresponding open loop zero-pole of Eq. (8) is obtained as shown in Fig. 2, in which, complex roots $\mathrm{p}_1 = -1/\tau_\mathrm{d} - \mathrm{j}\omega_\mathrm{s}$, $\mathrm{p}_2 = -1/\tau_\mathrm{s} - \mathrm{j}\omega_\mathrm{s}$, whose positions have relationships with the time constants τ_d and τ_s. When f_s is high, $\tau_\mathrm{s} >> \tau_\mathrm{d}$, the pole p_2 is the dominant one while p_1 has a little effect on the system performance. Reducing f_s makes p_1 be near to the zero shaft, and has a gradually enhanced influence on the system performance. Actually, the complex factor j in Eq. (8) is the essential reason why does the cross - coupling exists.

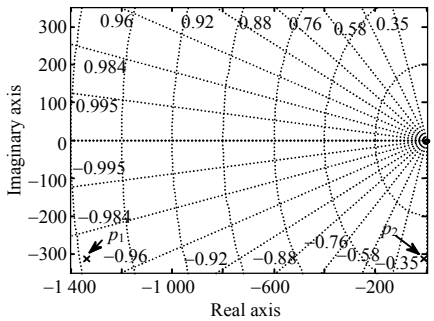

Fig. 2. Zero-Pole map of the unregulated open loop

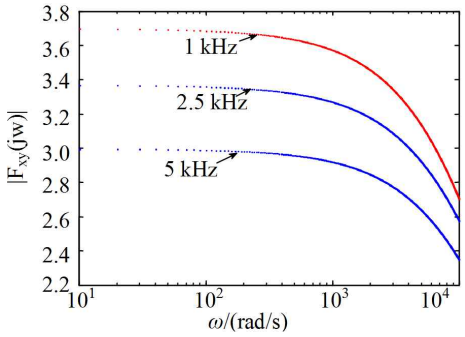

Fig. 3. Cross-coupling degree of the current loop at different switching frequency

In order to analyze the influence on cross-coupling in further, a coupling function in frequency domain is defined to describe the coupling degree.

$$\boldsymbol{F}_{xy}(\mathrm{j}\omega)=\frac{\mathrm{Im}\{\boldsymbol{F}(\mathrm{j}\omega)\}}{\mathrm{Re}\{\boldsymbol{F}(\mathrm{j}\omega)\}} \tag{9}$$

The coupling degree between i_d and i_q for this three-level PWM rectifier with a low switching frequency can be obtained by substituting Eq. (8) into Eq. (9), which is shown in Fig. 3. From Fig. 3, it can be seen that low switching frequency brings a more serious cross-coupling.

4. Complex Current Controller Design

4.1 Normal PI current controller

A normal PI with a feedforward compensation can realize the decoupling control for the current components i_d and i_q. For the complex transform of the current loop described as Eq. (5), a feedforward compensation $\mathrm{j}\omega_s\tau_s\boldsymbol{i}_s$ is introduced firstly, and then, a PI controller is given as

$$F_{\mathrm{PI}}(s)=k_0\frac{\tau_i s+1}{\tau_i s} \tag{10}$$

By designing k_0 and τ_i properly, the current loop can realize a nice control performance. However, with the consideration of a low switching frequency, extra cross-coupling, $\mathrm{j}\omega_s\tau_d\boldsymbol{i}_s$ exists as shown in Eq. (8). There are two parameters need to be adjusted along with double feedforward compensations if using normal PI control.

The Bode diagram and Step response of normal PI current with different switching frequency f_s are shown in Fig. 4.

From Fig. 4 (a), it can be known that the control bandwidth will reduce along with the decrease of the switching frequency, while the rising time, peak time, adjusting time and overshoot increase shown in Fig. 4 (b), which mean that normal current controller doesn't suitable

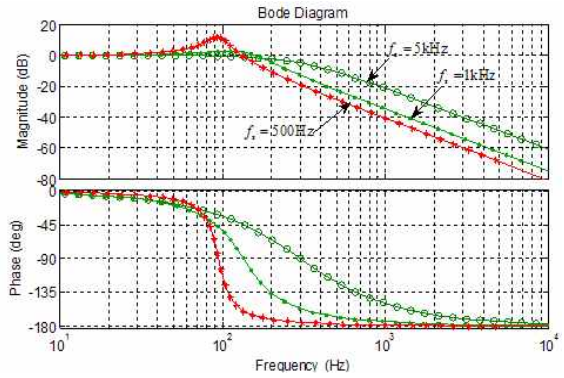

(a)

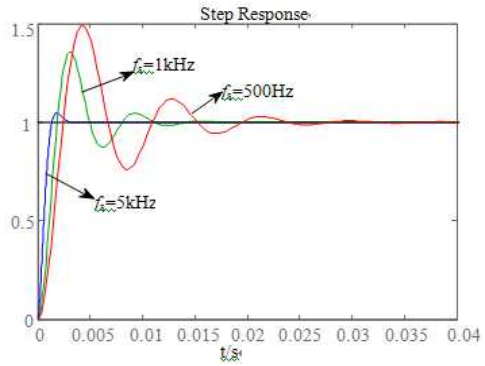

(b)

Fig. 4. Influence on normal current controller with different switching frequency: (a) Bode analysis; (b) Step response

anymore with a low switching frequency.

By tuning the gain value K_{iP} of the PI controller can get good performance without considering the switching frequency, as shown in Figs. 5(a) and 5(b). However, when the switching frequency is low, the adjustment of gain tuning can't improve the system performance to a great degree compared with the complex current controller. The comparisons between the normal PI controller and the complex one are shown in Fig.6 when f_s = 500 Hz (both of which have achieved the best effect).

4.2 Complex current controller design

From above theoretical analysis, we know that cross-coupling has closely relationship with imaginary parts existing in the complex transform. Given that a novel controller $F_r(s)$ designed to emit two complex poles at the same time, the coupling phenomenon would be eliminated fundamentally.

In this paper, $F_r(s)$ is re-designed as Eq. (11), which is also called a complex current controller.

$$F_{\mathrm{r}}(s)=k_0\frac{(\tau_s s+1+\mathrm{j}\omega_s\tau_s)(\tau_d s+1+\mathrm{j}\omega_s\tau_d)}{\tau_s s(\tau_d s+1)} \tag{11}$$

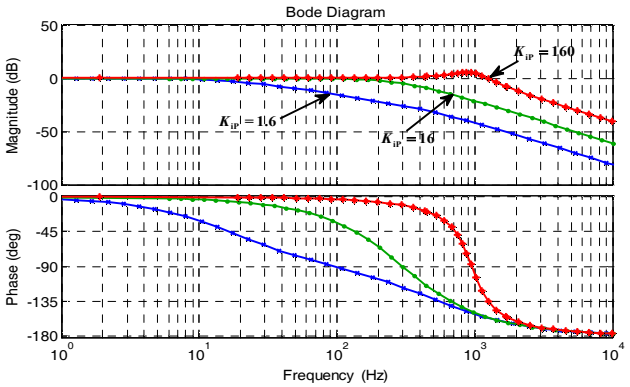

(a)

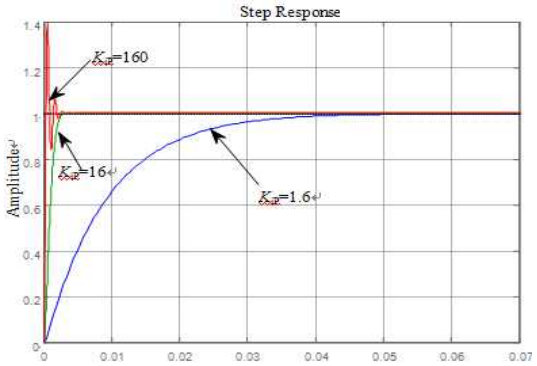

(b)

Fig. 5. Influence on normal current controller with different gain value (a) Bode analysis; (b) step response

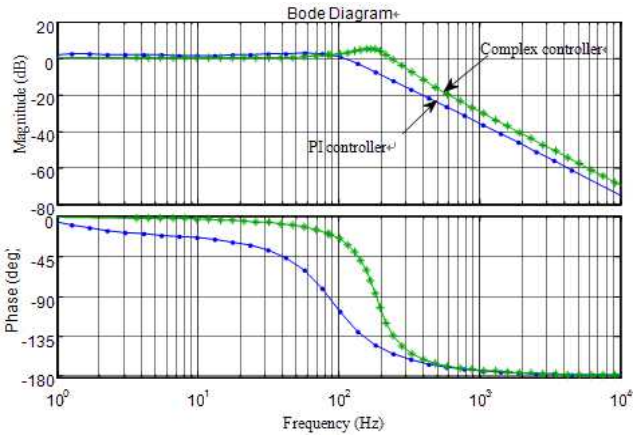

Fig. 6. Comparisons between the normal PI controller and the complex one

Where, there is only one parameter k_0 need to be designed and the complex signal graph of the current control system is shown in Fig. 7.

Substituting (11) into (8), the open loop current transform with a complex controller can be obtained as

$$F_o(s) = k_0 \frac{1}{\tau_s s(\tau_d s + 1)} \tag{12}$$

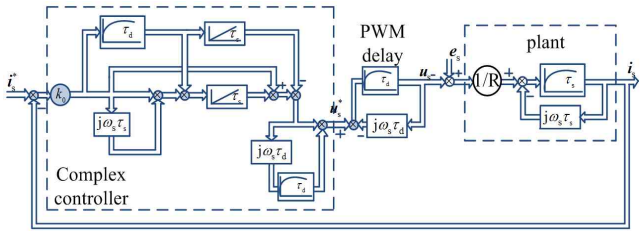

Fig. 7. Complex signal flow graph of the current control system with a complex current controller

Both complex poles now are eliminated and the coupling issue is solved.

In order to design the parameter k_0, a closed loop transform with current controller is given as

$$\begin{aligned} G(s) &= \frac{F_o(s)}{1+F_o(s)} = \frac{k_0/(\tau_s\tau_d)}{s^2 + (1/\tau_d)s + k_0/(\tau_s\tau_d)} \\ &= \frac{\omega_n^2}{s^2 + 2\xi\omega_n s + \omega_n^2} \end{aligned} \tag{13}$$

Where, $2\xi\omega_n = 1/\tau_d$, $\omega_n^2 = k_0/(\tau_s\tau_d)$.

Eq. (13) shows that this kind of closed loop is a typical second order system, whose damping coefficient ζ should be designed as 0.707 to reach an optimal performance [17], and then, the theoretical k_0 should be designed as

$$k_0 = \tau_s/(2\tau_d) \tag{14}$$

Considering the parameters of the three-level PWM rectifier are: amplitude of e_s is 690V, L = 5mH, R = 0.1 Ω, $C_1 = C_2$ = 6800μF, V_{dc} = 1800V, R_L = 0.1 Ω, f_s=500Hz, so the calculated τ_s = 0.05 and τ_d = 0.0015, the theoretical k_0 is 16.67, and the influence for different k_0 is shown in Fig. 8.

From Fig. 8, it can be seen that, larger k_0 can brings a more broad control bandwidth and a faster response, however, the overshoot increases. Fig. 8 gives a recommendation that k_0 in this paper is 20, which also verify the robustness of the designed complex current controller.

4.3 Simulation comparisons

The whole control scheme is designed as shown in Fig. 9, in which, the PI controller is used to control the DC-link voltage V_{dc}. The power factor is set as Pf =1 with taking the output of the PI voltage controller as the given value of i_d and the given value of i_q setting as zero.

Simulation comparisons have been carried out in MATLAB/simulink according to the control scheme as shown in Fig. 9, between the normal PI controller and the complex one while f_s = 500Hz, and a conventional PI controller is used for voltage outer loop. The simulation parameters are as same as the ones in the part 5; at t = 0s, R_L = 500Ω, at t =1.2s, R_L=100Ω.

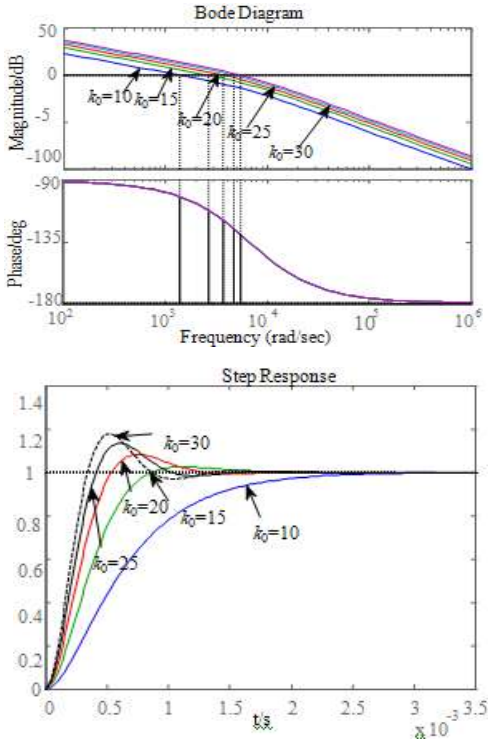

Fig. 8. Influence on the control system with different k_0

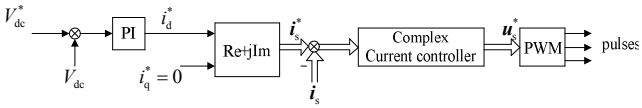

Fig. 9. Whole control scheme of the proposed strategy

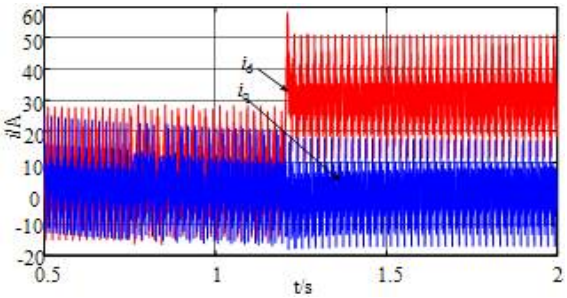

(a) normal PI controller

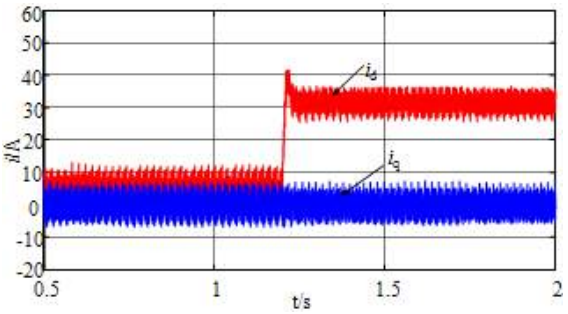

(b) complex current controller

Fig. 10. Current components i_d and i_q with different current controllers

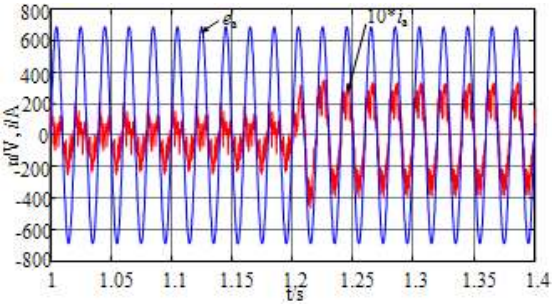

(a) normal PI controller

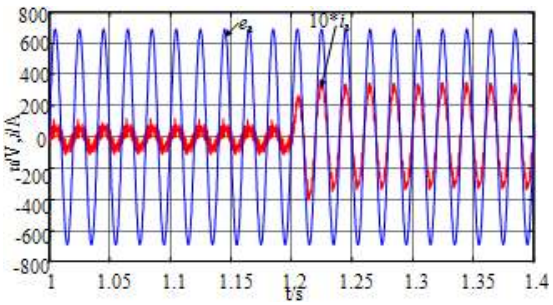

(b) complex current controller

Fig. 11. Grid voltage e_a and the enlarged grid-side current i_a with different current controllers

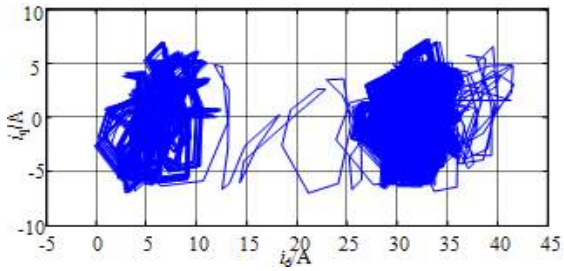

Fig. 12. Current trajectory of the grid-side current with the complex current controller

The current components i_d and i_q are shown in Fig. 10, the grid voltage e_a and the enlarged grid-side current i_a are shown in Fig. 11, Fig. 12 is the current trajectory of the grid-side current with the complex current controller.

From Fig. 10, it can be known that, this kind of complex current controller can realize the decoupling with a better characteristic compared with the normal PI controller. The harmonic distortion of grid-side current i_a also has been improved as shown in Fig. 11. The dynamic current trajectory shown in Fig. 12 verifies that this kind of complex controller has a nice dynamic performance.

5. Experimental Verification

Experimental platform has been established as shown in Fig. 13, where, a TI TMS320F28335 DSP is used to realize the control algorithm and a Xilinx Spartan3E-FPGA is

Table 1. Detail experimental parameters

Parameters	Value	Parameters	Value
Rated power(kW)	10	Grid voltage (V)	100
DC link voltage(V)	300	f_s(Hz)	500
filter inductance(H)	0.005	DC capacitor(μF)	6800
filter resistance(Ω)	0.1	Load (Ω)	100

Fig. 13. Experimental platform

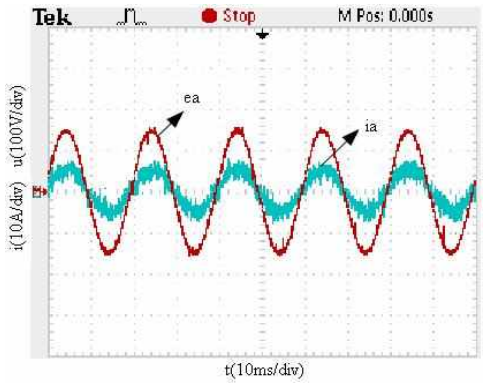

(a) normal PI

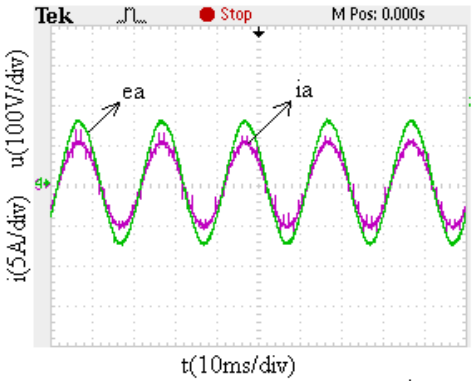

(b) complex current controller

Fig. 14. The grid voltage e_a and the grid-side i_a with different control strategy

adopted to implement A/D,D/A, pulses generation. Type of the Power devices is Infineon 450A, 1700V IGBT, whose drivers are the type of Concept (3W, 20A). The detailed scale of the experimental platform is shown in Table 1.

The implementation of the complex current controller is the most challenging part during the digital implementation. Firstly, Eq. (11) can be decomposed into the real and imaginary components. According to the definition in Eq. (3), that a real component corresponds the direct-axis one (d coordinate) while an imaginary part corresponds the quadrature axis one (q coordinate). Then, the complex current controller could be designed in dq coordinates.

The steady waveforms of grid voltage e_a and grid-side current i_a are shown in Fig. 14 with the different control strategy.

Fig. 14 shows that complex current controller has a better characteristic in reducing the harmonic distortion of the grid-side current.

During the experiment, the given V_{dc} = 300V, at t = 2s, V_{dc} = 450V and then reduced to 300V again. The corresponding DC-link voltage, current in dq coordinates are shown in Fig. 15. Sudden loading and unloading experimental results are shown in Fig. 16.

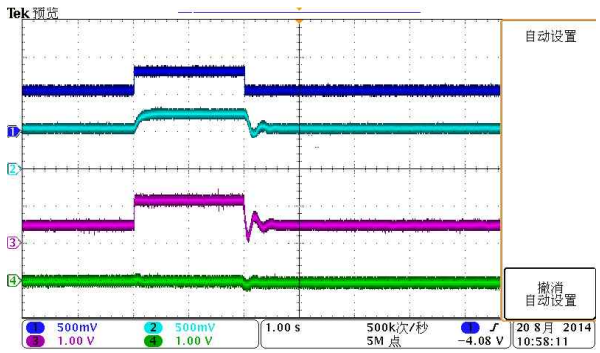

Fig. 15. Waveforms with a changement on the DC-link voltage, CH1: given DC-link voltage; CH2: real DC-link voltage; CH3: current of d coordinate; CH4: current of q coordinate

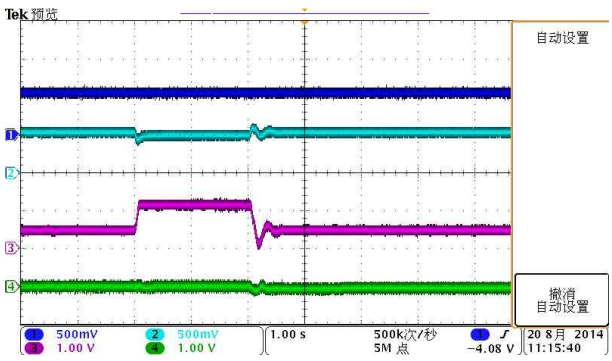

Fig. 16. Waveforms with a changement on the load, CH1: given DC-link voltage; CH2: real DC-link voltage; CH3: current of d coordinate; CH4: current of q coordinate

When a normal PI current controller was adopted, the dynamic waveforms of grid-side current i_a, the DC-link voltage V_{dc} and the current in dq coordinates are shown in Fig. 17 with the same experimental processes (the given V_{dc} = 300V, at t=2s, V_{dc}=450V and then reduced to 300V again), which is consistent with the simulation result shown in Fig. 10(a) and Fig. 11(a).

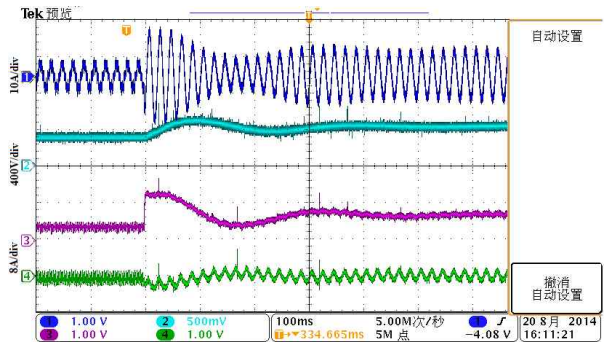

Fig. 17. Waveforms by PI controller CH1: grid-side current; CH2: real DC-link voltage; CH3: current of d coordinate; CH4: current of q coordinate

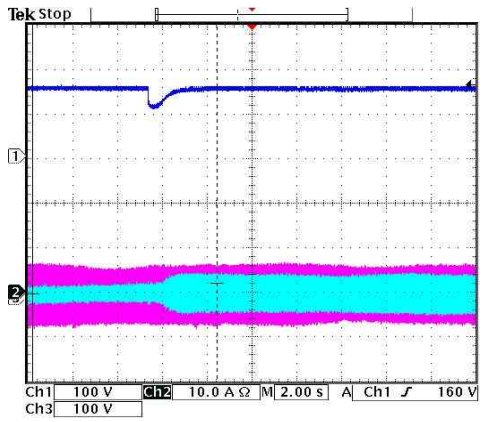

(a) Sudden loading

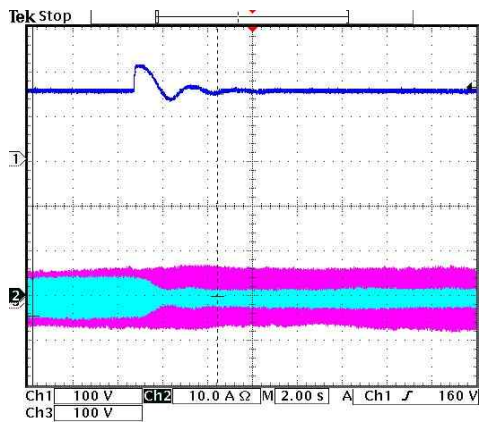

(b) Sudden unloading

Fig. 18. Experimental waveforms in dynamic state, CH1: DC-link voltage ; CH2: grid-side current i_a; CH3 grid voltage e_a

When the load changed suddenly, the dynamic grid voltage e_a and current i_a are shown in Fig.18 as well the dynamic DC-link voltage, which verify the dynamic performance of this kind of control scheme for three-level PWM rectifier.

6. Conclusions

Some research focusing on the decoupling control have been carried out for the three-level voltage source PWM rectifier considering a low switching frequency. Firstly, a novel complex model was established for the three-level PWM rectifier, and the influence resulted from low switching frequency was considered based on the detailed analysis on the influence on cross-coupling between in dq current components and performance of the normal current controller.

A complex current controller was proposed for the three-level PWM rectifier along with its parameter design, and the comparisons have been conducted between the normal PI current controller and the complex one.The whole control scheme was also given based on the microprocessors DSP and FPGA, and experiments were carried out to verify the effectiveness of the designed control system.

Acknowledgements

This work was supported by the National Natural Science Foundation of China (51207091/E070303) and the HuJiang Foundation of China (B14002/D14002) and the Shanghai Natual Science Foundation.

References

[1] J.A. Pontt et. al., "Network-friendly low-switching-frequency multipulse high-power three-level PWM rectifier," *IEEE Transactions on Industrial Electronics*, Vol.56, No.4, pp. 1254-1262, April.2009.

[2] H. Akagi et. al., "A new power line conditioner for harmonic compensation in power system," *IEEE Transactions on Power Delivery*, Vol.10, No.3, pp. 1570-1575, July.1995.

[3] Z. C. Zhang et. al., "Multimodular current-source SPWM converters for superconducting a magnetic energy storage system," *IEEE Transactions on Power Electronics*, Vol.8, No.3, pp.250-255,July.1993.

[4] C. Z. Javier et.al., "A large power, low switching frequency voltage source converter for FACTS applications with low effects on the transmission line," *IEEE Transactions on Power Electronics*, Vol. 27, No. 12, pp.4868-4879, Dec.2012.

[5] L. Cristian et.al., "Frequency response analysis of current controllers for selective harmonic compensa-

tion in active power filters," *IEEE Transactions on Industrial Electronics*, Vol. 56, No. 2, pp. 337-347, Feb. 2009.
[6] X. Q. Li et. al., "Stability analysis of grid-connected inverters with an LCL filter considering grid impedance," *Journal of Power Electronics*, Vol. 13, No. 5, pp. 896-908, Sept.2013.
[7] N. Oikonmou. *Control of medium-voltage drives at very low switching frequency*, Logos Verlag, 2008.
[8] L.G. Franquelo et.al., "New trends and topologies for high power industrial applications: The multilevel converters solution," *International Conference on Power Engineering, Energy and Electrical Drives*, pp. 1-6, 2009.
[9] A.G. Siemens. "Power semiconductors: for medium voltage converters-an overview," *13th European Conference on Power Electronics and Applications*, pp. 1-14, 2009.
[10] P. B. Rolando et.al., "Complex state variables modeling and nonlinear control of PWM voltage and current source rectifiers," *28th Annual Conference of the IEEE Industrial Electronics Society*, pp.187-192, 2002.
[11] J. Holtz et.al., "Design of fast and robust current regulators for high-power drives based on complex state variables," *IEEE Transactions on Industry Applications*, Vol. 40, No. 5, pp. 1388-1397, Sept.-Oct. 2004.
[12] J. Holtz et.al., "Estimation of the Fundamental Current in Low-Switching-Frequency High Dynamic Medium-Voltage Drives," *IEEE Transactions on Industry Applications*, Vol. 44, No. 5, pp. 1597-1605, Sept. -Oct. 2008.
[13] J. S. Liang et.al., "A three-phase PWM AC-DC converter with low switching frequency and high power factor using DSP-based repetitive control technique," *29th Annual IEEE Power Electronics Specialists Conferences*, pp.517-523, 1998.
[14] S. Kouro et.al., "Model predictive control - a simple and powerful method to control power converters," *IEEE Transactions on Industrial Electronics*, Vol. 56, No. 6, pp. 1826-1838, June. 2009.
[15] A. A. Rockhill et.al., "Grid-Filter Design for a Multimegawatt Medium-Voltage Voltage-Source Inverter," *IEEE Transactions on Industry Applications*, Vol. 58, No. 4, pp. 1205-1217, April. 2011.
[16] J. Holtz. "The representation of AC machine dynamics by complex signal flow graphs," *IEEE Transactions on Industrial Electronics*, Vol. 42, No. 3, pp. 263-271, Jun. 1995.
[17] B. S. Chen, *Automation control system for power drives*, China Machine Press, chap. 8, 2003.

Qing-qing YUAN She received her B.S., M.S. and Ph.D from the China University of Mining and Technology, China, in 2009, 2011, and 2014 respectively. Since 2014, she has been with the School of Optical-Electrical and Computer Engineering, University of ShangHai for Science and Technology, China, where she is currently a teacher. her current research interests include the modeling and control of high power drives with a low switching frequency.

Kun XIA He received his B.S., M.S. and Ph.D from the Hefei University of Technology, China, in 2002, 2004, and 2007 respectively. Since 2007, He is working as a teacher in Electrical Department, School of Optical-Electrical and Computer engineering, University of Shanghai for Science and Technology (USST) from July 2007 up to now. He is acting as the department dean and the leader of the electric professor group. He focused his main research work on electric engineering including motor control and new energy technology application.